A statistical study of the cross-shock electric potential at low Mach number, quasi-perpendicular bow shock crossings using Cluster data

A.P. Dimmock, M.A. Balikhin, V.V. Krasnoselskikh, S.N. Walker, S.D. Bale, Y Hobara

A statistical study of the cross-shock electric potential at low Mach number, quasi-perpendicular bow shock crossings using Cluster data

A. P. Dimmock,[1] M. A. Balikhin,[1] V. V. Krasnoselskikh,[2] S. N. Walker,[1] S. D. Bale,[3] and Y. Hobara[4]

Received 22 August 2011; revised 7 November 2011; accepted 17 December 2011; published 21 February 2012.

[1] The cross-shock electrostatic potential at the front of collision-less shocks plays a key role in the distribution of energy at the shock front. Multipoint measurements such as those provided by the Cluster II mission provide an ideal framework for the study of the cross-shock potential because of their ability to distinguish between temporal and spacial variations at the shock front. We present a statistical study of the cross-shock potential calculated for around 50 crossings of the terrestrial bow shock. The statistical dependency of the normalized (with resect to upstream ion kinetic energy) cross-shock potential (Φ_K) on the upstream Alfvén Mach number is in good agreement with analytical results that predict decrease of Φ_k with increasing Mach number.

Citation: Dimmock, A. P., M. A. Balikhin, V. V. Krasnoselskikh, S. N. Walker, S. D. Bale, and Y. Hobara (2012), A statistical study of the cross-shock electric potential at low Mach number, quasi-perpendicular bow shock crossings using Cluster data, *J. Geophys. Res.*, *117*, A02210, doi:10.1029/2011JA017089.

1. Introduction

[2] The physics of collisionless shocks is one of the fundamental areas of plasma physics research. The main process that takes place at the shock front is the redistribution of the kinetic energy from supersonic bulk flow into other degrees of freedom [*Sagdeev*, 1966; *Sagdeev and Galeev*, 1969; *Papadopoulos*, 1985]. In strong, quasi-perpendicular and supercritical planetary bow shocks the macro field structure that results from structures such as the cross-shock potential, has a greater effect on the energy redistribution processes than the various micro instabilities [*Scudder et al.*, 1986; *Walker et al.*, 2008].

[3] Studies of the magnetic field profile across the terrestrial bow shock significantly outnumber those based on electric field measurements. Despite the fundamental effect that the electric field has on the plasma dynamics across collisionless shocks, the complexity of the interpretation of electric field data has impeded studies of the electric field structure within the shock front. While hundreds of papers are devoted to the magnetic field structure of collisionless shocks [e.g., *Russell et al.*, 1983; *Farris et al.*, 1991; *Newbury and Russell*, 1996; *Hobara et al.*, 2010] only a handful of studies are dedicated to the electric field structure within the shock front [*Heppner et al.*, 1978; *Formisano*, 1982; *Scudder et al.*, 1986; *Wygant et al.*, 1987; *Balikhin et al.*, 2002; *Walker et al.*, 2004; *Balikhin et al.*, 2005; *Bale and Mozer*, 2007; *Hobara et al.*, 2008; *Dimmock et al.*, 2011; S. D. Bale et al., Direct measurement of the cross-shock electric potential at low plasma β, quasi-perpendicular bow shocks, 2008, http://arxiv.org/abs/0809.2435]. The computation of the cross-shock potential (Φ) is non-trivial since it requires the spatial integration of the electric field across the shock. These calculations are particularly sensitive to the errors introduced by factors such as bad estimates of the shock normal direction, and the relative shock/spacecraft velocity. Multispacecraft missions such as Cluster are well suited to the study of cross-shock potential since they provide the means for the distinction between temporal and spatial variations.

[4] One major problem with electric field measurements is that the component of the electric field measured perpendicular to the spin plane is either measured using a short antenna length (e.g. Polar, Geotail) or is not measured at all e.g. Cluster. Parallel and perpendicular electric fields were studied by *Bale and Mozer* [2007] where $E_{\parallel}$ was calculated directly using the 3-axis measurements of the Polar spacecraft. However, for cases when the spin axis component is unavailable, several methods have been used to calculate cross-shock potential. The first assumes that if the angle between the spin plane and the shock normal is small then an accurate value for the potential can be estimated using only the two measured components [*Balikhin et al.*, 2002]. A second method was proposed by Bale et al. (arXiv eprint, 2008) where the normal component of the electric field was

[1]Department of Automatic Control and Systems Engineering, University of Sheffield, Sheffield, UK.
[2]Laboratoire de Physique et Chimie de l'Environnement et de l'Espace, Orleans, France.
[3]Physics Department and Space Sciences Laboratory, University of California, Berkeley, California, USA.
[4]Department of Communication Engineering and Informatics, University of Electro-Communications, Tokyo, Japan.

0148-0227/12/2011JA017089

constructed based on the assumption that the cross-shock potential lies along the normal direction. A third method estimates the missing electric field component using the ideal Magnetohydrodynamic (MHD) condition $\mathbf{E} \cdot \mathbf{B} = 0$. However, while this assumption can be true in some regions of the magnetosphere it is definitely not valid within the quasi-perpendicular shock front. The existence of an electric field component directed along the magnetic field at the shock front has been shown in experimental studies such as those by *Scudder et al.* [1986]. The existence of flat topped electron distributions with a superimposed beam realigned downstream of the shock front has been interpreted as evidence that $\mathbf{E} \cdot \mathbf{B} \neq 0$ within the shock [*Feldman et al.*, 1983]. Recently a fourth method based on the electric field structure in the Normal Incident Frame (NIF) has been proposed by *Dimmock et al.* [2011]. All calculations are performed in the following LMN shock co-ordinate system in which the first axis (N) lies along the normal ($\hat{\mathbf{n}}$), the second axis (M) is perpendicular to both $\hat{n}$ and the upstream magnetic field direction ($\mathbf{B_{Up}}$), and the final axis (L) completes the right handed set. The electric field in the NIF is the combination of two non-zero sources, namely an electrostatic component due to the shock potential

$$\mathbf{E_\Phi} = -\nabla\Phi \tag{1}$$

and a component due to the motion of the plasma.

$$\mathbf{E_m} = -\frac{1}{c}\mathbf{V_m} \times \mathbf{B_{Up}} \tag{2}$$

Above, $\mathbf{V_m} = V_{Sh} + V_M$ is the sum of shock velocity directed along the normal (V_{Sh}), and the NIF frame velocity given by

$$\mathbf{V_N} = \hat{\mathbf{n}} \times \left(\mathbf{V_{Up}} \times \hat{\mathbf{n}}\right) \tag{3}$$

where $\mathbf{V_{Up}}$ is the upstream plasma velocity. The NIF electric field is therefore given by:

$$\mathbf{E_{NIF}} = \mathbf{E_\Phi} + \mathbf{E_m} \tag{4}$$

For shocks in the quasi-perpendicular regime, magnetic field may be resolved into 2 components directed parallel ($B_\parallel$) and perpendicular ($B_\perp$) to the shock normal. Since velocity of the plasma in the NIF is directed along the shock normal, only $B_\perp$ will contribute to $\mathbf{E_m}$. Therefore from equations (1), (2), (3) and (4):

$$\mathbf{E_{NIF}} \cdot \mathbf{B}_\perp = 0 \tag{5}$$

Equation (5) allows the reconstruction of $\mathbf{E_{NIF}}$ which provides the means to determine Φ. The cross-shock potential is obtained by the spatial integral of $\mathbf{E_{NIF}}$ along the shock normal i.e. $E_N = \mathbf{E_{NIF}} \cdot \hat{\mathbf{n}}$

$$\Phi = \int_P E_N \, ds \tag{6}$$

where s represents the spatial co-ordinates of E_N along the path defined by P which starts just prior to the foot and terminates at the end of the identified ramp.

[5] The purpose of this paper is to investigate the dependency between the cross-shock electrostatic potential, and the parameters of the quasi-perpendicular bow shock such as the Alfvén Mach number (M_A) and the angle between the normal and the upstream magnetic field (Θ_{Bn}). We present a statistical study of the cross-shock electric potential for around 50 crossings of the terrestrial bow shock observed by the Cluster spacecraft between 2001 and 2008. The following section will discuss the data sets and instrumentation used to complete the work before moving on to discuss three examples of shocks that were analyzed during this study. Finally the results of the statistics will be interpreted prior to discussing the scientific interpretations.

2. Data and Instrumentation

[6] All the statistical data gathered for this study were collected by the Cluster spacecraft [*Escoubet et al.*, 1997] between 2001 to 2008. From the abundance of shock crossings available during this period, 44 crossings by all four spacecraft (138 individual crossings) were used to make up the statistical data set for this study. The selection criteria for the shocks will be outlined in the next section. Electric field data, used to estimate the cross-shock potential, were collected by the Electric Fields and Waves experiment (EFW) [*Gustafsson et al.*, 1997], which is part of the wave consortium controlled by the Digital Wave Processor (DWP) [*Woolliscroft et al.*, 1997]. The electric field sensors, used by the EFW instrument consist of four spherical probes each of which is attached to the satellite via a 44m wire boom. The potential difference between opposing pairs of probes provides an estimate of the electric field for the x and y components within the inverted spacecraft spin frame (ISR2). The ISR2 frame differs from the Geocentric Solar Ecliptic frame (GSE) by <6° because the spin axis is tilted slightly to reduce shadowing of the electric field probes. The limitations imposed by the EFW instrument require the reconstruction of the missing electric field component. In this case, the unavailable z component is determined based on a technique reliant upon the structure of the electric field in the NIF [*Dimmock et al.*, 2011].

[7] The shock crossing times are identified using measurements recorded by the Fluxgate Magnetometers (FGM) onboard each of the 4 Cluster satellites [*Balogh et al.*, 1997]. Ion density (N_i), used to calculate the M_A, was estimated using the electron plasma frequency (ω_{pe}) measured by the WHISPER instrument [*Décréau et al.*, 1997]. The solar wind upstream bulk flow velocity ($\mathbf{V_{up}}$) was obtained from measurements taken by the Cluster Ion Spectrometer (CIS) [*Rème et al.*, 1997]. In some instances where CIS data were either unavailable or unreliable, propagated solar wind measurements made by the Solar Wind Electron, Proton, and Alpha Monitor (SWEPAM) [*McComas et al.*, 1998] instrument onboard ACE were used. This was achieved by correlating magnetic field measurements made by the ACE magnetic field experiment (MFI) [*Smith et al.*, 1998] with the Cluster FGM data set to determine the propagation time. All upstream solar wind velocities were validated using measurements of the upstream ion energy from the CIS instrument.

3. Bow Shock Crossing Measurements

[8] Shocks were initially chosen based on the availability and the quality of the FGM and EFW measurements. As

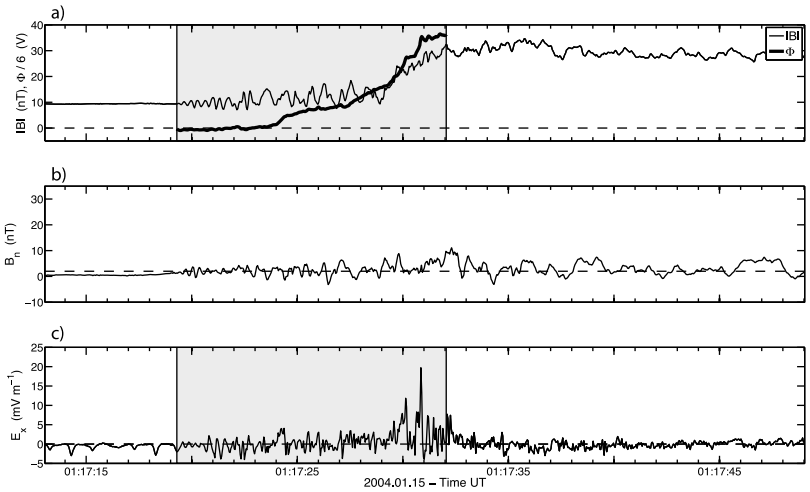

Figure 1. A shock crossing made by the Cluster spacecraft on 2004.01.15 01:17 UT. (a) The magnitude of the magnetic profile of the shock crossing plotted with Φ. (b) B_n. (c) E_x in the spacecraft spin frame.

these conditions were verified, the most critical condition was the ability to obtain an accurate shock normal direction since this has a direct impact on the potential estimates. The impact on the potential as a result of a variation of a 10° cone around the normal was investigated by *Dimmock et al.* [2011]. These authors showed that there could be significant variation in the calculated values of the potential. Their results suggested that for the particular shock studied, a change in the normal direction of 10° yielded a change in potential by 20 %. All shock normal ($\hat{\mathbf{n}}$) directions were identified using the model shock surface by *Farris et al.* [1991], minimum variance analysis [*Sonnerup and Cahill*, 1967] or the multispacecraft technique [*Schwartz*, 1998]. The resulting normal directions were compared in order to ensure a consistent and reliable direction for the normal. In some cases where multispacecraft analysis was unreliable (due to large spacecraft separation) minimum variance analysis was used. There is no such method that will guarantee 100 % accuracy of the shock normal determination. Therefore, to estimate the possible errors relating to the identification of the normal, error analysis is performed by introducing a 10° deviation about $\hat{\mathbf{n}}$. The velocity along the shock normal (V_{Sh}) was determined based on a selection of the spatial separation vectors (S) of the four Cluster satellites as they encountered the bow shock. The angles between the S vectors and $\hat{\mathbf{n}}$ were used as the criteria for identifying the optimal satellite pairings based on the condition they were not close to perpendicular. If the separation vectors and $\hat{\mathbf{n}}$ are close to perpendicular then a minor timing inaccuracy could possibly result in large variations of V_{Sh}. The plausibility and variation of the velocities of each separation vector along $\hat{\mathbf{n}}$ were also taken into consideration. V_{Sh} was determined by computing the mean of the velocities of the chosen separation vectors along $\hat{\mathbf{n}}$. In a number of cases where multiple spacecraft cross the terrestrial bow shock over a short time interval, neither CIS or WHISPER measurements were available from all four spacecraft. In such cases M_A is calculated using plasma data from the closest crossing.

[9] Three example shocks will be discussed to demonstrate the analysis methods and assumptions used for each of the chosen shock crossings. The first illustrates a typical example that lies within the selection criteria. The second example shows a case where V_{Sh} is very high(> 150 kms^{-1}) and thus does not provide good structural detail during the shock. This shock was omitted due to possible errors in the potential estimate. The third example shows a shock which was omitted due to the inability to determine an accurate shock normal direction.

3.1. Shock 1: 15 January 2004, 01:17 UT

[10] Figure 1 displays a shock crossing recorded by the Cluster 3 (C_3) spacecraft on 15 February 2004. Figure 1a shows the magnitude of the magnetic field profile and the cross-shock potential estimation (thick line). Figure 1b shows the magnetic field directed along the normal. Figure 1c shows the x component of the electric field in the ISR2 frame. This particular shock was observed at 01:17 UT and was one of several shocks that occurred on this day. Solar wind conditions were normal on this day with upstream measurements made by the CIS instrument providing a solar wind flow velocity of 519 kms^{-1}. Measurements made upstream by the Cluster 1 FGM indicated $|\mathbf{B_{up}}|$ to be approximately 9.2 nT. The model normal direction was [0.90, 0.37 −0.21], and was validated using the multispacecraft normal, the two directions differing by ≈7°. The variation of B_n shows minimal variation during the shock region (≈5 nT) providing further confidence in the direction of the shock normal, whereas the change in the magnitude observed during the ramp crossing is approximately 25–30 nT. The difference in the average upstream and far downstream normal component of the magnetic field is also insignificant, providing greater confidence in $\hat{\mathbf{n}}$. The crossings made by the C_1, C_2 and C_4 spacecraft are not shown here since they are very similar to that observed by C3 however, they are well represented by Figure 1. The geometry of the shock was quasi-perpendicular ($\Theta_{bn} \approx 88°$). The plasma density was estimated using WHISPER electron frequency measurements as $N_i = 6.3$ cm^{-1}, resulting in an Alfvén velocity $V_a \approx 75.5$ km s^{-1} and $M_a \approx 6.3$. The supercritical nature of the shock is further supported by the well defined foot, ramp, and overshoot characteristics seen in

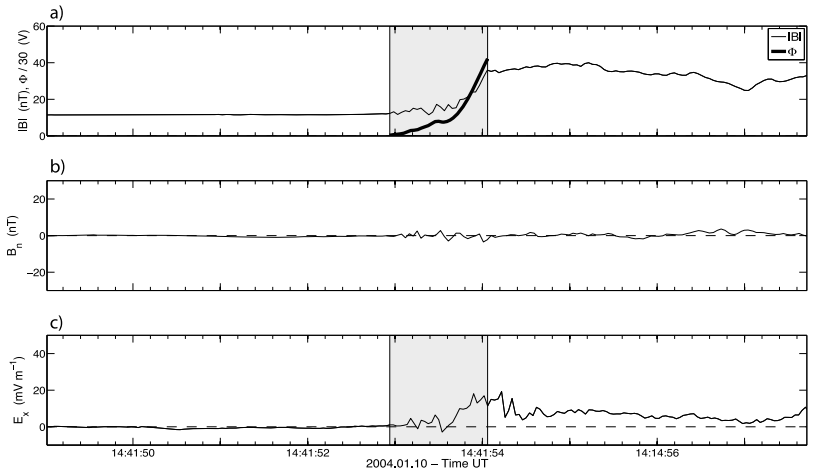

Figure 2. A shock crossing made by the Cluster spacecraft on 2004.01.10, 17:05 UT. (a) The magnitude of the magnetic field profile of the shock crossing plotted with Φ. (b) B_n. (c) E_x in the spacecraft spin frame.

Figure 1a. The order in which the bow shock passed over the satellites was C_1, C_2, C_3 and C_4. V_{Sh} was determined from the mean of the velocity component along the normal calculated using the three pairs (S_{12}, S_{13} and S_{23}) whose spatial separation vectors were least perpendicular with $\hat{\mathbf{n}}$. In this case, $V_{Sh} \approx 16.8$ km s^{-1}. Figure 1c shows the EFW measurements (E_x) for the same period. Nonlinear structures with magnitudes of the order of 12 mVm^{-1} were observed in the electric field during the ramp crossing. A possible reason for the good structural detail measured across the shock may be due to the relatively slow shock-spacecraft velocity. The low frequency plasma waves in $|\mathbf{B}|$ observed prior to the ramp also correlate with an increase in electric field activity observed in E_x, which intensifies during the ramp then diminishes downstream. A statistical study of these small scale structures within the ramp of the terrestrial bow shock based on Cluster observations was performed by *Walker et al.* [2004]. These structures have been observed in the majority of electric field measurements during the crossings in this study. In some cases these small scale structures contribute 20 to 30 % of the total cross-shock potential.

[11] The profile of the electrostatic potential is consistent with that expected across a quasi-perpendicular shock. The illustration in Figure 1 shows zero potential prior to a steady increase coinciding with the foot region, the majority of the field is the result of the shock ramp, which displays the highest potential gradient. The foot typically contributes around 20 % of the total cross-shock potential. However, in some cases this can be substantially more depending on the amount of wave activity present prior to the ramp. The electric field structures intensify across the ramp and therefore the potential exhibits sharp increases which dominate the overall potential magnitude. It is worth noting that the increase in potential is often influenced by well defined small scale structures across the shock ramp. This is supported by the structures observed in both Φ and E_x in Figures 1a and 1c at 01:07:35 and 01:07:36 respectively. The estimates of the potential from each of the four spacecraft were scaled with respect to the upstream ion kinetic energy $\mathrm{K}_i^{up} = \frac{1}{2} M_i |V_{up}|^2$, ($\Phi_K$) and were 0.23, 0.26, 0.20 and 0.21 respectively. The consistency of Φ_K and the strong confidence in the shock parameters indicate this shock lies within the ideal criteria for shock selection.

3.2. Shock 2: 10 January 2004, 14:41 UT

[12] Figure 2 shows a shock crossing made by C_1 on 10 January 2004 at 14:14 UT using the same format as Figure 1. Cluster encountered this shock in the order C_1, C_2, C_3 and C_4. The model normal in this case was [0.88, 0.31, −0.34], which lies favorably with the normal resulting from multi-spacecraft timing analysis which varies by ≈11°. B_n shows a small variation within the shock ramp and no upstream/downstream change. Conditions upstream of the shock indicated a solar wind velocity of $|\mathbf{V_u}| = 656$ km s^{-1} and magnetic field of $|\mathbf{B_{up}}| = 11$ nT. The crossing was quasi-perpendicular in geometry as the angle between $\mathbf{B_{up}}$ and $\hat{\mathbf{n}}$ was $\Theta_{Bn} = 87°$. V_{Sh} was calculated using the three pairs of spacecraft separation vectors (S_{12}, S_{13}, S_{13}) that were the least perpendicular with $\hat{n}$. In this case the angles of the chosen separation vectors with $\hat{n}$ were [33°, 42°, 53°]. The mean velocity, based on the three separation vectors was calculated to be $V_{Sh} \approx 155$ kms^{-1}. According to WHISPER measurements, plasma density was $n_i = 7.8$ giving $M_A = 6.7$. The cross-shock potential (Figure 2a) still displays the expected profile for a perpendicular shock albeit over a smaller time duration due to a high V_{Sh}. The unusually high shock velocity should have significant implications on the measurements. Such a magnitude of velocity can be implicitly confirmed by the absence of short scale structures both in the foot, and ramp regions. The resulting cross-shock potentials calculated from all four spacecraft and scaled with respect to K_i^{up}, were [1.3, 1.9, 2.5, 2.0] for C_1, C_2, C_3 and C_4 respectively. The large values of the normalized potentials possibly result from the sparse sampling of the electric field within the shock front due to the high velocity at which the shock was encountered. This can lead to inaccuracies in the spatial integration of the electric field. For this reason, this shock was eliminated from the study.

3.3. Shock 3: 31 March 2001, 21:35 UT

[13] This particular shock was excluded because of the inability to determine an acceptable shock normal and due to

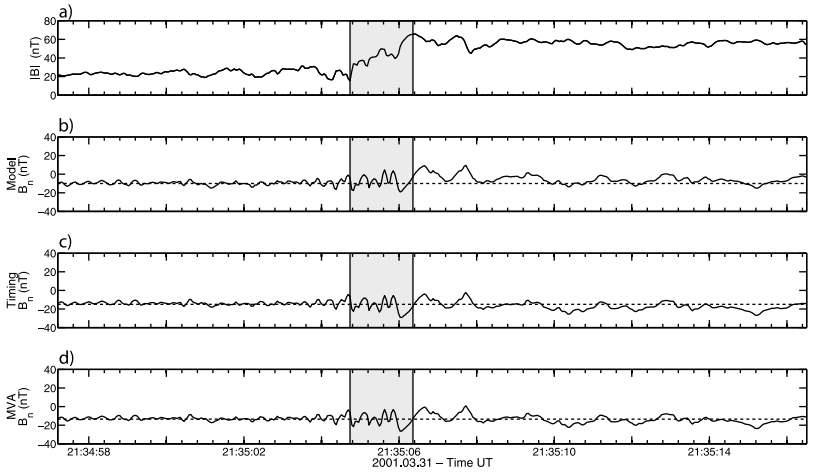

Figure 3. A crossing of the terrestrial bow shock made by Cluster 1 on 31 March 2001 at 21:35 UT. (a) The magnitude of the magnetic field profile. (b, c, d) The magnetic field directed along all the normal directions. Figures 3b, 3c, and 3d represent the model normal, multispacecraft timing normal and the minimum variance normals respectively.

an unexpectedly high V_{Sh}. On 31 March 2001 Cluster observed the passing of a CME and subsequently 11 crossings of the terrestrial bow shock were observed on this day. Figure 3 shows the crossing made by the C_1 spacecraft at 21:35 UT. The satellites encountered the shock in the order of C_4, C_2, C_1 and C_3. Upstream measurements gave a solar wind velocity of 587 kms^{-1} and magnetic field magnitude of 21 nT. The shock normal direction was determined using the model ($\hat{\mathbf{n}}$), multispacecraft analysis ($\hat{\mathbf{n}}_{\mathbf{sc}}$), and minimum variance ($\hat{\mathbf{n}}_{\mathbf{MV}}$) techniques which resulted in normal directions of [0.94, −0.14, 0.30], [0.85, −0.28, 0.45] and [0.88, −0.26, 0.40] respectively. The magnetic profile measured by C_1 can be seen in Figure 3a and its projection along the three normals in Figures 3b–3d. The normal directions show good agreement to within around 10°. However, there are fluctuations observed in B_n between 21:35:05 and 21:35:07 which are approximately 50 % of the ramp change in magnitude (40 nT). These large variations in B_n do not suggest a satisfactory normal determination. Based on the model normal and the optimal pairings of S_{23} and S_{34} the shock spacecraft velocity was 156 kms^{-1}. If the timing and minimum variance normals were used the resulting velocities were 109 kms^{-1} and 113 kms^{-1} respectively. Using WHISPER measurements, the Alfvén Mach number was determined to be 5.2.

[14] This section has discussed the processing for three separate shock crossings. The first met the selection criteria whereas the other two did not. Very high shock velocity can result in small inaccuracies being magnified later in the analysis. As V_{Sh} has a direct influence on cross-shock potential, shocks with velocity in excess of 150 kms^{-1} were not included in our results. If there is significant variation along B_n then shocks were also discarded. The conclusions derived from the results of this study only include shocks which met this criteria.

4. Results of the Cross-Shock Potential Estimations

[15] As was mentioned above, the main criteria for shock selection was based on the high reliability of the shock normal

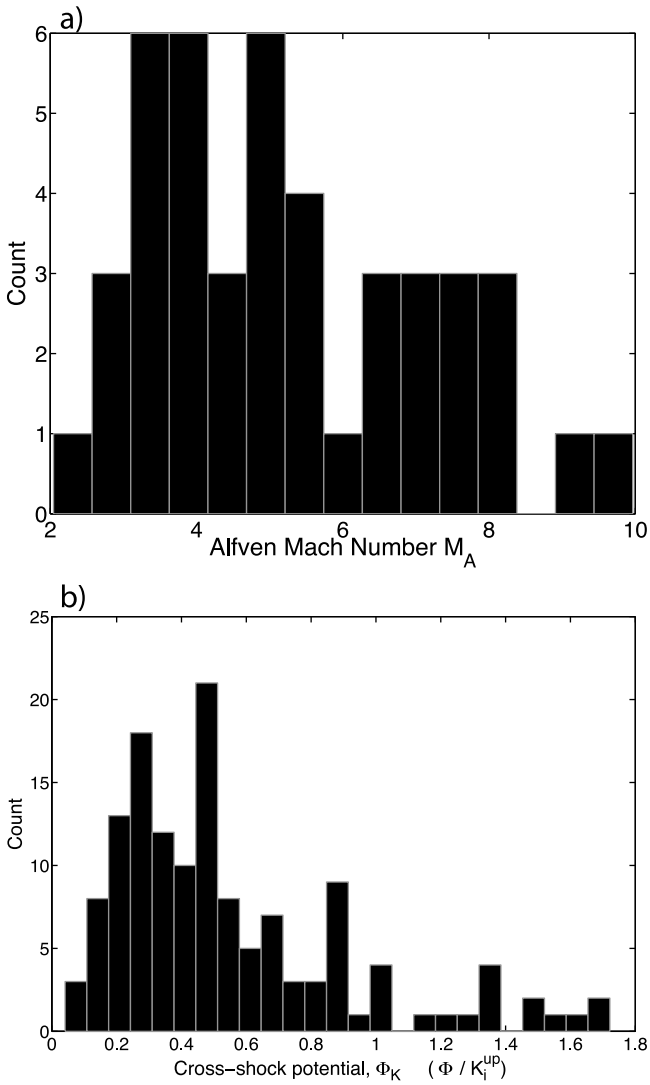

Figure 4. The distributions of (a) M_A and (b) Φ_k for all the included shocks.

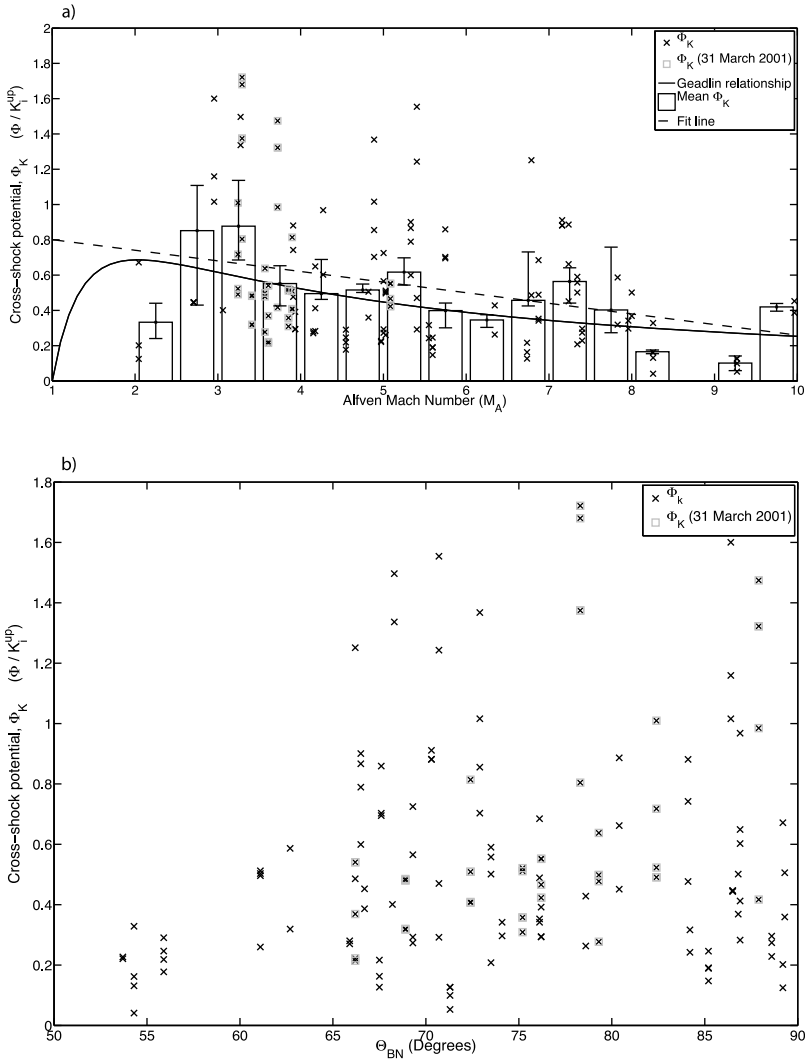

Figure 5. Scaled cross-shock potential plotted against (a) Alfvén Mach number and (b) Θ_{Bn} for 44 shocks (138 individual crossings) observed by the Cluster spacecraft between 2001 and 2008.

identification. This criterion was chosen since a badly identified normal direction has a critical effect on the estimation of the electrostatic potential. This appears to be a very strict criterion because only 44 shocks (138 spacecraft crossings) were selected from the abundance of crossings that were recorded by the Cluster spacecraft during the time period from 2001 to 2008. Figure 4 represents the distribution of M_A (Figure 4a) and estimated electrostatic potential (Figure 4b) normalized using the upstream ion kinetic energy. For the majority of cases, M_A falls between 3 and 6, which is expected from crossings of the terrestrial bow shock [*Kennel et al.*, 1985]. As expected, Figure 4b suggests that for most of the crossings, the magnitude of Φ is below the value of the upstream ion kinetic energy. For the majority of cases the cross-shock potential consists of contributions from both the foot and ramp regions of the shock transition. In almost all cases the ramp results in the largest magnitude of the electric field and the greatest contribution to the overall magnitude of the electrostatic potential. The foot region ordinarily accounts for around 20% of the total value of the electrostatic potential ($|\Phi|$), as is demonstrated in Figure 2a. However, for some shocks this contribution can be even greater as was observed during the shock crossing shown in Figure 1a in which the foot provides nearly 40% of $|\Phi|$. In many cases, electric field structures which occur over small spatial scales within the ramp can also contribute around 20% to the overall potential estimate. When present, these spike like structures nearly always occur during the ramp region, such as shown in Figure 1b at 01:17:30.5. In this particular case, the electric field peaks at approximately 20mVm^{-1} which, regardless of its small spatial scale, is notably larger than any of the other electric field structures measured in the vicinity of the shock crossing (shaded area).

[16] Figures 5 and 6 display Φ_k and Φ plotted against M_A (Figures 5a and 6a) and Θ_{Bn} (Figures 5b and 6b) respectively. The bars displayed in Figure 5a represent the averaged Φ_k using Mach number bins of width 0.5 in the range 2 to 10 (i.e. 2–2.5,.. ,9.5–10). The upper and lower limits of the error bars for values of Φ_k represent the maximum and minimum values of the potential computed assuming a 10 degree

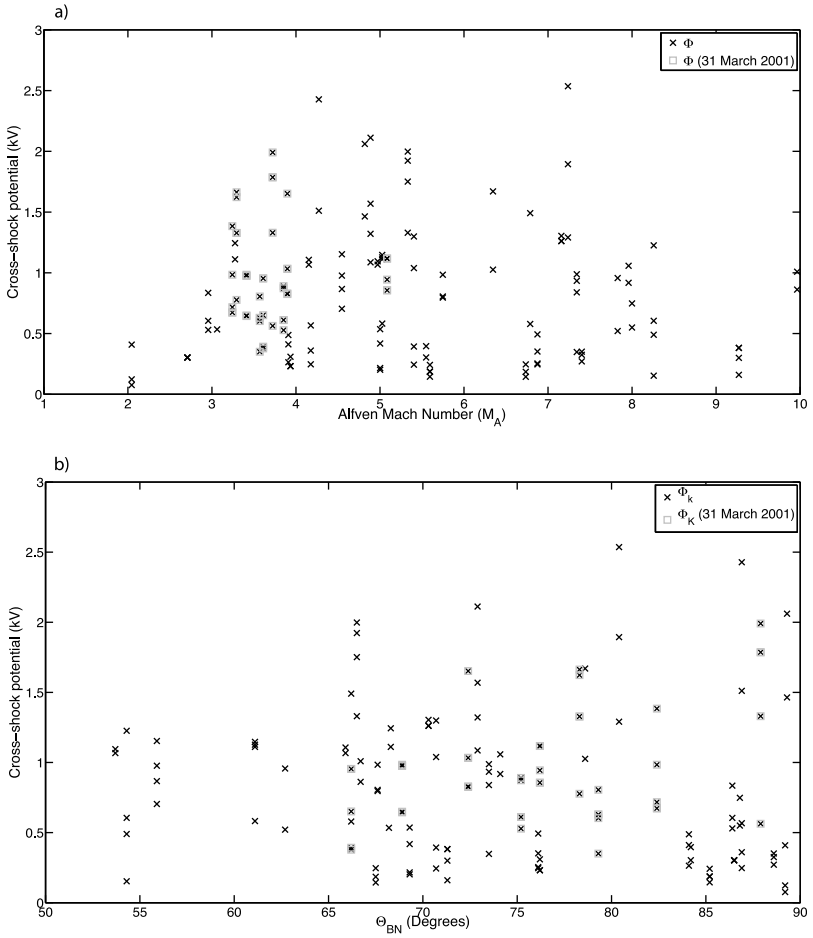

Figure 6. Directly calculated cross-shock potential plotted against (a) Alfvén Mach number and (b) Θ_{Bn} for 44 shocks (138 individual crossings) observed by the Cluster spacecraft between 2001 and 2008.

variation in the direction of the shock normal. The cross-shock potential error Φ_e consists of both upper and lower limits which represent the estimated variation of Φ resulting from the normal variance.

$$\Phi_e = \Phi \pm (\Phi_{\min}, \Phi_{\max}) \tag{7}$$

Above, $\Phi_{\min}$, and $\Phi_{\max}$ represent the maximum and minimum changes in potential resulting from the error analysis. Therefore the upper and lower limits of the error bars illustrated in Figure 5 are determined by calculating the means of the statistical data set using both the maximum and minimum values of Φ_e. The dashed line represents the linear best fit for all values of the potential determined in this study. The solid line in Figure 5 represents the analytical relationship by *Gedalin* [1997]

$$\Phi_k = \frac{|\Phi|}{K_i^{up}} = \frac{2(B_d/B_u - 1)}{{M_a}^2} \tag{8}$$

derived from Ohms law which relates the normalized cross-shock potential (Φ_k) to the upstream Mach number (M_a) where B_d, B_u are the upstream and downstream magnetic fields respectively.

[17] Figures 4, 5, and 6 show that even though a strict selection criteria was used for the shocks in this study, there is still a significant variation in the magnitude of the electrostatic potential. It would be expected that the statistical data set would exhibit some large variations in the electrostatic potential. However, it is interesting that Figures 5 and 6 suggest that there is a substantial variation in the electrostatic potential between spacecraft measurements of the same shock crossings. This is unexpected since in most cases the spatial separation of the satellites was of the order of hundreds of km. In a study performed by Bale et al. (arXiv eprint, 2008), the estimated cross-shock potential for the 10 shocks observed on 31 March 2001 also showed a significant variation between different spacecraft. Since Bale et al. (arXiv eprint, 2008) applied a different methodology for the reconstruction of the electric field, these differences cannot arise from the new methods applied in this study. Possible physical reasons for the variation in potential could be the slight change of direction in the shock normal between spacecraft. However, the error bars suggest that normal inaccuracy (or misidentification) alone cannot result in a large enough change in $|\Phi|$ to account for some shocks. The variation in some cases has to be attributed to the non stationarity of the shock, which cannot be ignored when considering multispacecraft measurements.

[18] Figures 5b and 6b suggest that as the shock geometry becomes closer to perpendicular, the range of values of electrostatic potential increases. This may imply that the more perpendicular the shock front, the more susceptible it is to non-stationarity. Figure 5a indicates that the normalized cross-shock potential has a tendency to decrease as M_A increases. This relationship is also proposed by Gedalin's analytical expression. The means displayed in Figure 5a show a striking resemblance to the characteristics of Gedalin's equation. This suggests that the trend shown in the experimental data is similar in nature to the analytical result. In support of this, the magnitude and gradient of the line of best fit also closely follow the analytical solution. The magnitude of the statistical results do not exactly match the analytical work. However, this is not surprising since the analytical expression was derived on the basis of several assumptions which could account for this difference. These will be considered in more detail later. Both the peak of Φ_k at lower mach numbers (2–4), and the general decrease of the normalized electrostatic potential thereafter are clearly evident. It is worth mentioning that there are some unexpected increases in the mean bars such as in the ranges of 5–5.5 and 7–7.5. However, some variation would be expected in the statistical results due to data set outliers, and the significant variation of potential due to shock non-stationarity. Regardless of this, the general trend of the data indicated by the means, individual points and the fitted line suggest that there is sufficient clarity to draw reliable conclusions from these results.

5. Discussion

[19] Equation (8) was derived based on the following assumptions: 1) massless electrons, 2) adiabatic electrons, 3) $n \propto B$ and $p_e \propto B^2$, 4) the domination of an electron current, and 5) low plasma β. While assumption 1 is expected to be a good approximation for all heliospheric shocks, the remaining three may not be completely valid. Electron adiabaticity is expected to be violated in the electric field spikes [*Balikhin and Gedalin*, 1994; *Gedalin et al.*, 1995] where the second approximation could not be satisfied. Yet, when the electrons are demagnetized, the perpendicular electron current also becomes suppressed [*Gedalin et al.*, 1995] which results in a slower increase of the magnetic field, so that the error due to the demagnetization is diminished. Such a decrease in the magnetic field growth associated with simultaneously observed short scale spikes in the electric field is often observed in satellite data [e.g., *Balikhin et al.*, 2002]. It can be seen from Figure 1a that stronger gradients in the electrostatic potential caused by the two electric field spikes within the magnetic ramp observed around 01:17:30 and 01:17:31 coincide with considerable decreases of the magnetic field gradient. The approximation $n \propto B$ and $T \propto B$ are, strictly speaking, only valid for perpendicular geometry, yet for sufficiently large angles between the shock normal and the upstream magnetic field deviations are weak. The electron current clearly dominates in the structures with large magnetic field gradients such as the ramp, but this effect is drastically reduced in the foot where the reflected ion current is important. In the shocks with a developed foot, equation (8) should be applied to the ramp only. Given the number of approximations and observational uncertainties, the agreement (at the statistical level) between the resulting trend and the theoretically predicted dependency on M_A is striking.

[20] Ion reflection is known to occur above the second critical Mach number. As a result, this study suggests that the shock parameters on the macroscopic scale are closely related to the non-adiabatic deceleration of the ions at the shock front. A possible reason for the decrease in normalized potential with increasing M_A is that the increase in cross-shock potential may prove too strong to allow ion reflection [*Wilkinson and Schwartz*, 1990] and so reduce the number and energy of the directly transmitted ions [*Gedalin*, 1996a]. However, the number of ions escaping would be expected to increase with increasing Mach number [*Gedalin et al.*, 2008], to provide the required dissipation to prevent overturning.

[21] The variance of $|\Phi_k|$ displayed in Figures 5 and 6 could be due to several factors. First, shock non-stationarity can result in unexpectedly high potential estimates. This can also cause large ranges of the Φ resulting from multipoint measurements. This process is also believed to be somewhat responsible for the existence of the small spatial scale electric field structures within the shock ramp. Secondly, the presence of helium ions which possess a larger mass can lead to elevated estimates of cross-shock potential at the shock front. Finally, substantial dispersion of the obtained values for the cross-shock potential may be related to the difficulties in the determination of the shock normal for supercritical shocks where the downstream ion distributions are noticeably non gyrotropic. As a result, the non-coplanar component of the magnetic field [*Gedalin*, 1996b] is significant, and the coplanarity theorem is not valid in the near vicinity of the ramp. The possible error of the shock normal has been considered and is illustrated by error bars in Figure 5 however, this alone cannot be responsible for the distribution of the cross-shock potential in some cases which means some other process such as the above must be responsible.

[22] The electrostatic cross-shock potential can significantly differ between frames of reference. *Goodrich and Scudder* [1984] considered this frame dependence and concluded that Φ is considerably smaller when calculated in the de Hoffmann-Teller frame. They also conclude that the electrostatic potential is typically of the same order of magnitude as the upstream ion kinetic energy. The implications of this suggest that the NIF is the more appropriate choice of frames when considering the work performed by the ions at the quasi-perpendicular shock front. Our results also suggest that for the vast amount of terrestrial bow shock crossings in the quasi-perpendicular regime, the electrostatic potential is less than the upstream ion kinetic energy (see Figure 5).

[23] To summarize, cross-shock potential is one of the fundamental parameters that controls the redistribution of the upstream ion kinetic energy at the quasi-perpendicular shock front. Due to the technical challenges typically associated with its calculation, studies of cross-shock potential on a statistical basis are very limited. The results presented here support conclusions of previous work such as the analytically derived equation (8) for the cross-shock potential. Another important conclusion from these results is that a substantial contribution to the overall cross-shock potential comes from the short scale electric field structures shown in Figure 1. The fact that on most occasions the change of

electrostatic potential is far from uniform, and includes significant contributions from very short spacial scale electric field structures, implies the contribution of non adiabatic effects to the electron thermalization process within the shock front. Notably, the variance of the cross-shock potential seen in Figures 4, 5 and 6 can represent the manifestation of shock non-stationarity.

[24] **Acknowledgments.** This work was supported by STFC and EPSRC grants. The authors wish to acknowledge the CAA teams for providing the data sets for this study.

[25] Philippa Browning thanks the reviewers for their assistance in evaluating this paper.

References

Bale, S. D., and F. S. Mozer (2007), Measurement of large parallel and perpendicular electric fields on electron spatial scales in the terrestrial bow shock, *Phys. Rev. Lett.*, *98*(20), 205001, doi:10.1103/PhysRevLett.98.205001.

Balikhin, M., and M. Gedalin (1994), Kinematic mechanism of electron heating in shocks: Theory vs observations, *Geophys. Res. Lett.*, *21*, 841–844, doi:10.1029/94GL00371.

Balikhin, M., S. Walker, R. Treumann, H. Alleyne, V. Krasnoselskikh, M. Gedalin, M. Andre, M. Dunlop, and A. Fazakerley (2005), Ion sound wave packets at the quasiperpendicular shock front, *Geophys. Res. Lett.*, *32*, L24106, doi:10.1029/2005GL024660.

Balikhin, M. A., et al. (2002), Observation of the terrestrial bow shock in quasi-electrostatic subshock regime, *J. Geophys. Res.*, *107*(A8), 1155, doi:10.1029/2001JA000327.

Balogh, A., et al. (1997), The cluster magnetic field investigation, *Space Sci. Rev.*, *79*, 65–91.

Décréau, P. M. E., P. Fergeau, V. Kranoselskikh, M. LévÊque, P. Martin, O. Randriamboarison, F. X. Sené, J. G. Trotignon, P. Canu, and P. B. Mögensen (1997), Whisper, a resonance sounder and wave analyser: performances and perspectives for the cluster mission, *Space Sci. Rev.*, *79*, 157–193.

Dimmock, A. P., M. A. Balikhin, and Y. Hobara (2011), Comparison of three methods for the estimation of cross-shock electric potential using cluster data, *Ann. Geophys.*, *29*(5), 815–822, doi:10.5194/angeo-29-815-2011.

Escoubet, C. P., R. Schmidt, and M. L. Goldstein (1997), Cluster: Science and mission overview, *Space Sci. Rev.*, *79*, 11–32, doi:10.1023/A:1004923124586.

Farris, M. H., S. M. Petrinec, and C. T. Russell (1991), The thickness of the magnetosheath: Constraints on the polytropic index, *Geophys. Res. Lett.*, *18*, 1821–1824, doi:10.1029/91GL02090.

Feldman, W. C., R. C. Anderson, S. J. Bame, S. P. Gary, J. T. Gosling, D. J. McComas, M. F. Thomsen, G. Paschmann, and M. M. Hoppe (1983), Electron velocity distributions near the earth's bow shock, *J. Geophys. Res.*, *88*, 96–110, doi:10.1029/JA088iA01p00096.

Formisano, V. (1982), Measurement of the potential drop across the earth's collisionless bow shock, *Geophys. Res. Lett.*, *9*, 1033–1036, doi:10.1029/GL009i009p01033.

Gedalin, M. (1996a), Transmitted ions and ion heating in nearly perpendicular low-Mach number shocks, *J. Geophys. Res.*, *101*, 15,569–15,578, doi:10.1029/96JA00924.

Gedalin, M. (1996b), Noncoplanar magnetic field in the collisionless shock front, *J. Geophys. Res.*, *101*, 11,153–11,156, doi:10.1029/96JA00518.

Gedalin, M. (1997), Ion heating in oblique low-mach number shocks, *Geophys. Res. Lett.*, *24*, 2511–2514, doi:10.1029/97GL02524.

Gedalin, M., K. Gedalin, M. Balikhin, V. Krasnosselskikh, and L. J. C. Woolliscroft (1995), Demagnetization of electrons in inhomogeneous E⊥B: Implications for electron heating in shocks, *J. Geophys. Res.*, *100*, 19,911–19,918, doi:10.1029/95JA01399.

Gedalin, M., M. Liverts, and M. A. Balikhin (2008), Distribution of escaping ions produced by non-specular reflection at the stationary quasi-perpendicular shock front, *J. Geophys. Res.*, *113*, A05101, doi:10.1029/2007JA012894.

Goodrich, C. C., and J. D. Scudder (1984), The adiabatic energy change of plasma electrons and the frame dependence of the cross-shock potential at collisionless magnetosonic shock waves, *J. Geophys. Res.*, *89*, 6654–6662, doi:10.1029/JA089iA08p06654.

Gustafsson, G., et al. (1997), The electric field and wave experiment for the cluster mission, *Space Sci. Rev.*, *79*, 137–156, doi:10.1023/A:1004975108657.

Heppner, J. P., N. C. Maynard, and T. L. Aggson (1978), Early results from ISEE-1 electric field measurements, *Space Sci. Rev.*, *22*, 777–789.

Hobara, Y., et al. (2008), Cluster observations of electrostatic solitary waves near the Earth's bow shock, *J. Geophys. Res.*, *113*, A05211, doi:10.1029/2007JA012789.

Hobara, Y., M. Balikhin, V. Krasnoselskikh, M. Gedalin, and H. Yamagishi (2010), Statistical study of the quasi-perpendicular shock ramp widths, *J. Geophys. Res.*, *115*, A11106, doi:10.1029/2010JA015659.

Kennel, C. F., J. P. Edmiston, and T. Hada (1985), A quarter century of collisionless shock research, in *Collisionless Shocks in the Heliosphere: A Tutorial Review*, *Geophys. Monogr. Ser.*, vol. 34, edited by R. G. Stone and B. T. Tsurutani, pp, 1–36, AGU, Washington, D. C.

McComas, D. J., S. J. Bame, P. Barker, W. C. Feldman, J. L. Phillips, P. Riley, and J. W. Griffee (1998), Solar Wind Electron Proton Alpha Monitor (SWEPAM) for the Advanced Composition Explorer, *Space Sci. Rev.*, *86*, 563–612, doi:10.1023/A:1005040232597.

Newbury, J. A., and C. T. Russell (1996), Observations of a very thin collisionless shock, *Geophys. Res. Lett.*, *23*, 781–784, doi:10.1029/96GL00700.

Papadopoulos, K. (1985), Microinstabilities and anomalous transport, in *Collisionless Shocks in the Heliosphere: A Tutorial Review*, *Geophys. Monogr. Ser.*, vol. 34, edited by R. G. Stone and B. T. Tsurutani, pp. 59–90, AGU, Washington, D. C.

Rème, H., et al. (1997), The cluster ion spectrometry (CIS) experiment, *Space Sci. Rev.*, *79*, 303–350.

Russell, C. T., M. M. Mellott, E. J. Smith, and J. H. King (1983), Multiple spacecraft observations of interplanetary shocks Four spacecraft determination of shock normals, *J. Geophys. Res.*, *88*, 4739–4748, doi:10.1029/JA088iA06p04739.

Sagdeev, R. Z. (1966), Cooperative phenomena and shock waves in collisionless plasmas, *Rev. Plasma Phys.*, *4*, 23–90.

Sagdeev, R. Z., and A. A. Galeev (1969), *Nonlinear Plasma Theory*, W.A. Benjamin, New York.

Schwartz, S. J. (1998), Shock and discontinuity normals, mach numbers, and related parameters, *ISSI Sci. Rep. Ser.*, *1*, 249–270.

Scudder, J. D., T. L. Aggson, A. Mangeney, C. Lacombe, and C. C. Harvey (1986), The resolved layer of a collisionless, high beta, supercritical, quasi-perpendicular shock wave: 1. Rankine-Hugoniot geometry, currents, and stationarity, *J. Geophys. Res.*, *91*, 11,019–11,052, doi:10.1029/JA091iA10p11019.

Smith, C. W., J. L'Heureux, N. F. Ness, M. H. Acuña, L. F. Burlaga, and J. Scheifele (1998), The ACE magnetic fields experiment, *Space Sci. Rev.*, *86*, 613–632, doi:10.1023/A:1005092216668.

Sonnerup, B. U. O., and L. J. Cahill Jr. (1967), Magnetopause structure and attitude from Explorer 12 observations, *J. Geophys. Res.*, *72*, 171–183, doi:10.1029/JZ072i001p00171.

Walker, S. N., H. S. C. K. Alleyne, M. A. Balikhin, M. André, and T. S. Horbury (2004), Electric field scales at quasi-perpendicular shocks, *Ann. Geophys.*, *22*, 2291–2300.

Walker, S. N., M. A. Balikhin, H. S. C. K. Alleyne, Y. Hobara, M. André, and M. W. Dunlop (2008), Lower hybrid waves at the shock front: a reassessment, *Ann. Geophys.*, *26*, 699–707, doi:10.5194/angeo-26-699-2008.

Wilkinson, W. P., and S. J. Schwartz (1990), Parametric dependence of the density of specularly reflected ions at quasi-perpendicular collisionless shocks, *Planet. Space Sci.*, *38*, 419–435, doi:10.1016/0032-0633(90)90108-3.

Woolliscroft, L. J. C., H. S. C. Alleyne, C. M. Dunford, A. Sumner, J. A. Thompson, S. N. Walker, K. H. Yearby, A. Buckley, S. Chapman, and M. P. Gough (1997), The digital wave-processing experiment on cluster, *Space Sci. Rev.*, *79*, 209–231.

Wygant, J. R., M. Bensadoun, and F. S. Mozer (1987), Electric field measurements at subcritical, oblique bow shock crossings, *J. Geophys. Res.*, *92*, 11,109–11,121, doi:10.1029/JA092iA10p11109.

S. D. Bale, Physics Department and Space Sciences Laboratory, University of California, Berkeley, CA 94720-7450, USA.

M. A. Balikhin, A. P. Dimmock, and S. N. Walker, Department of Automatic Control and Systems Engineering, University of Sheffield, Sheffield S1 3JD, UK. (a.dimmock@sheffield.ac.uk)

Y. Hobara, Department of Communication Engineering and Informatics, University of Electro-Communications, Tokyo 182-8585, Japan.

V. V. Krasnoselskikh, LPC2E, 3A Ave. de la Recherche Scientifique, F-45071 Orleans, France.